Supplementary information: Investigation of the role of morphology on the magnetic properties of $Ca_2Mn_3O_8$ materials

Laura J. Vera Stimpson,[1] Silvia Ramos,[1] Gavin B. G. Stenning,[2] Marek Jura,[2] Stephen Parry,[3] Giannantonio Cibin[3] and Donna C. Arnold[1]

[1] *School of Physical Sciences, University of Kent, Canterbury, Kent, CT2 7NH, UK*

[2] *ISIS Neutron and Muon Source, Rutherford Appleton Laboratory, Harwell Science and Innovation Campus, Didcot, OX11 0QX, UK*

[3] *Diamond Light Source, Harwell Science and Innovation Campus, Didcot, Oxfordshire OX11 0DE, UK*

Refinement details

All refinements were performed using the GSAS suite of programs[1,2] and the model proposed by Ansell *et al.*[3] for 36 variables including zero-point and 18-term shifted Chebyshev background coefficients. Peak shape was refined by employing a pseudo-Voight function and spherical harmonic (ODF) coefficients were refined for the hydrothermally prepared $Ca_2Mn_3O_8$ in order to model for preferred orientation.

Results and Discussion

Structural Analysis

Figure S1 gives the Rietveld refinement profiles for the hydrothermal and co-precipitation synthesised $Ca_2Mn_3O_8$ materials (please note the refinement profile for the Sol-gel synthesised material is shown in the main body of the article). Table S1 gives a summary of the refined parameters. Table S2 gives a summary of the bond lengths and bond angles determined from Rietveld refinement for each of the materials. Figure S2 shows an expanded region of the normalised absorption (from figure 4 in the main body of the article) for all samples and standards showing that normalisation are consistent across all materials. Figures S3(a) and (b) shows a comparison of the EXAFS data in reciprocal (k) and real space respectively for all three data samples. It is evident from these plots that the local structure is identical for all three morphologies with the exception of the effects of disorder. The fitted EXAFS data for the hydrothermal and co-precipitation prepared $Ca_2Mn_3O_8$ materials is shown in figure S4 and further confirms that a single model can be used to fit to all samples.

Note the EXAFS fits for the Sol-gel prepared material is shown in the main body of the article.

Table S1: *Rietveld refinement parameters for the refinement of powder X-ray diffraction data collected for hydrothermal, co-precipitation and sol-gel synthesised $Ca_2Mn_3O_8$ materials fitted using the monoclinic C2/m model.*[3]

Parameter	Sol-gel	Hydrothermal	Co-precipitation
w*Rp* (%)	6.67	4.68	8.59
***Rp* (%)**	5.28	3.67	6.80
a (Å)	11.059(2)	11.023(1)	11.037(1)
b (Å)	5.8605(9)	5.8537(7)	5.8452(6)
c (Å)	4.9560(7)	4.9613(4)	4.9505(5)
β (º)	109.78(1)	109.662(8)	109.752(8)
Cell Volume (Å³)	302.26(8)	301.46(5)	300.59(5)
Ca (*x*,0,*y*)	0.729(2) 0.668(4)	0.7200(7) 0.658(2)	0.7221(9) 0.669(2)
Mn1 (0,0,½)	-	-	-
Mn2 (0,*y*,0)	0.264(2)	0.254(2)	0.265(1)
O1 (*x*,*y*,*z*)	0.101(5) 0.222(7) 0.396(7)	0.098(1) 0.223(2) 0.400(3)	0.100(1) 0.230(3) 0.390(3)
O2 (*x*,½,*z*)	0.591(8) 0.93(2)	0.599(2) 0.901(5)	0.597(3) 0.917(7)
O3 (*x*,0,*z*)	0.622(7) 0.96(2)	0.592(2) 0.916(6)	0.604(3) 0.954(7)

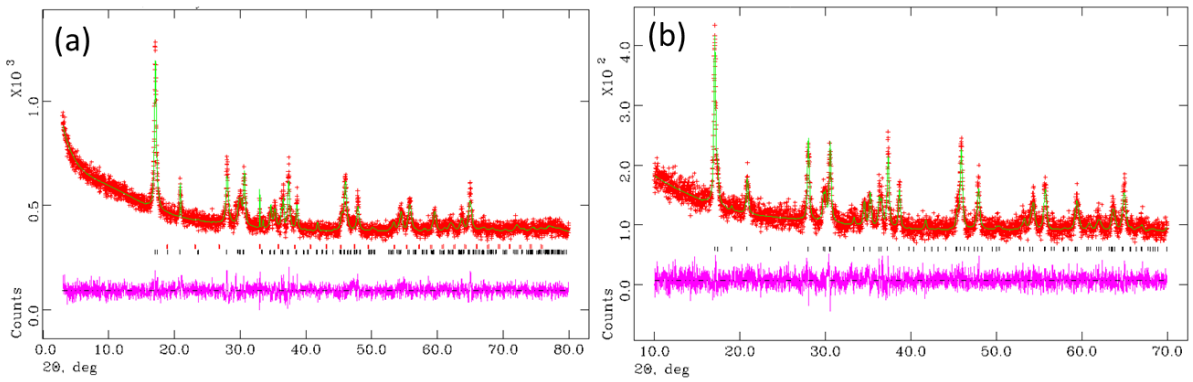

Figure S1: *Rietveld refinement profiles for data fitted using the monoclinic C2/m model [3] to powder X-ray diffraction data collected for $Ca_2Mn_3O_8$ prepared (a) hydrothermally and (b) by sol-gel methods. The red circles represent the observed data, the green line represents the calculated model and the pink line represents the difference.*

Table S2: *Bond lengths and selected bond angles extracted from the Rietveld refinement of powder X-ray diffraction data collected for hydrothermal, co-precipitation and sol-gel synthesised $Ca_2Mn_3O_8$ materials fitted using the monoclinic C2/m model.*[3]

Bond lengths (Å)	**Sample**		
	Sol-gel	**Hydrothermal**	**Co-precipitation**
Mn_1 - O_1 (x4)	1.91(5)	1.87(1)	1.93(1)
Mn_1 - O_2 (x2)	2.01(9)	1.92(2)	1.98(3)
Mn_2 - O_1 (x2)	1.92(3)	1.92(2)	1.88(2)
Mn_2 - O_2 (x2)	1.95(6)	2.00(1)	2.00(1)
Mn_2 - O_3 (x2)	1.98(5)	1.89(1)	1.86(2)
Ca - O_1 (x2)	2.39(4)	2.49(1)	2.48(1)
Ca - O_1 (x2)	2.27(5)	2.22(1)	2.23(1)
Ca - O_2	2.30(8)	2.42(2)	2.33(3)
Ca - O_3	2.17(9)	2.20(2)	2.22(3)
Mn_1-O_1-Mn_2	99(3)	99.5(7)	100.0(8)
Mn_1-O_2-Mn_2	95(3)	95.2(7)	94(1)
Mn_2-O_2-Mn_2	105(4)	96(1)	101(1)
Mn_2-O_3-Mn_2	88(3)	99(1)	96(1)

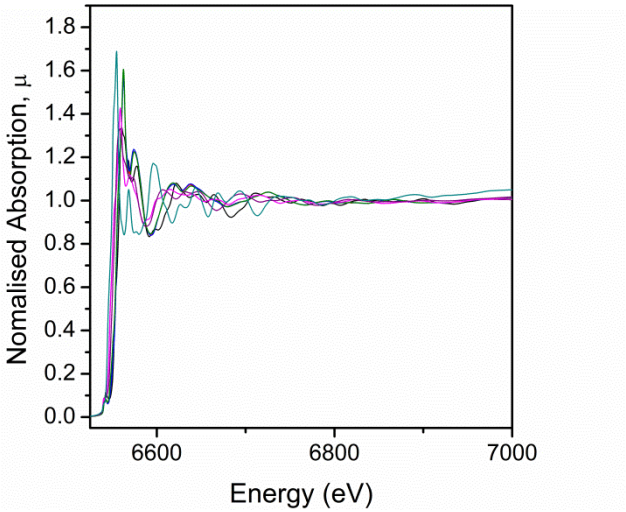

Figure S2: *Normalised Mn K-edge XANES spectra showing the edge position of $Ca_2Mn_3O_8$ materials prepared by sol-gel (red), co-precipitation (blue) and hydrothermal (green) methods are consistent with MnO_2 (black) and thus an oxidation state of +4 in comparison with Mn_3O_4 (magenta), Mn_2O_3 (purple) and MnO (dark cyan). This plot shows an expanded range from that shown in the manuscript confirming that the normalisation is consistent across all materials.*

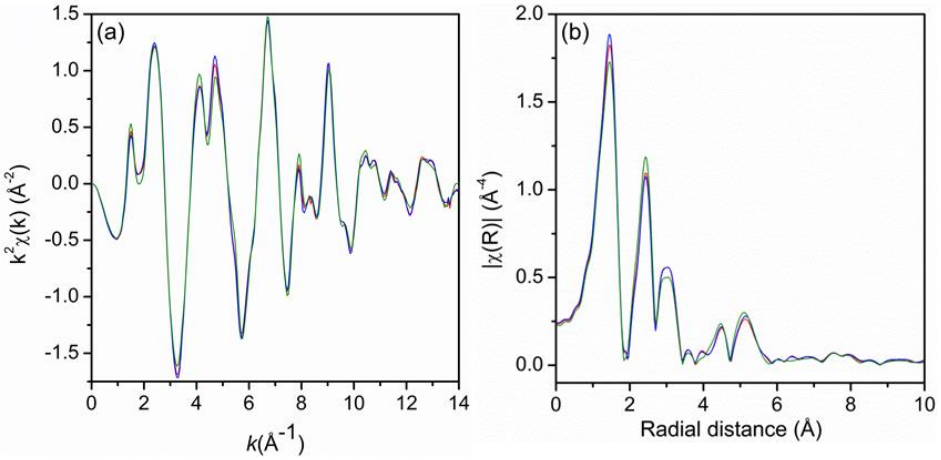

Figure S3: *Comparison of the EXAFS spectra for the $Ca_2Mn_3O_8$ materials prepared by sol-gel (red), co-precipitation (blue) and hydrothermal (green) indicating that the local structure is the same irrespective of morphology and synthetic route. Data are shown in (a) reciprocal (k) space and (c) the real component of the EXAFS Fourier transform in real space (R).*

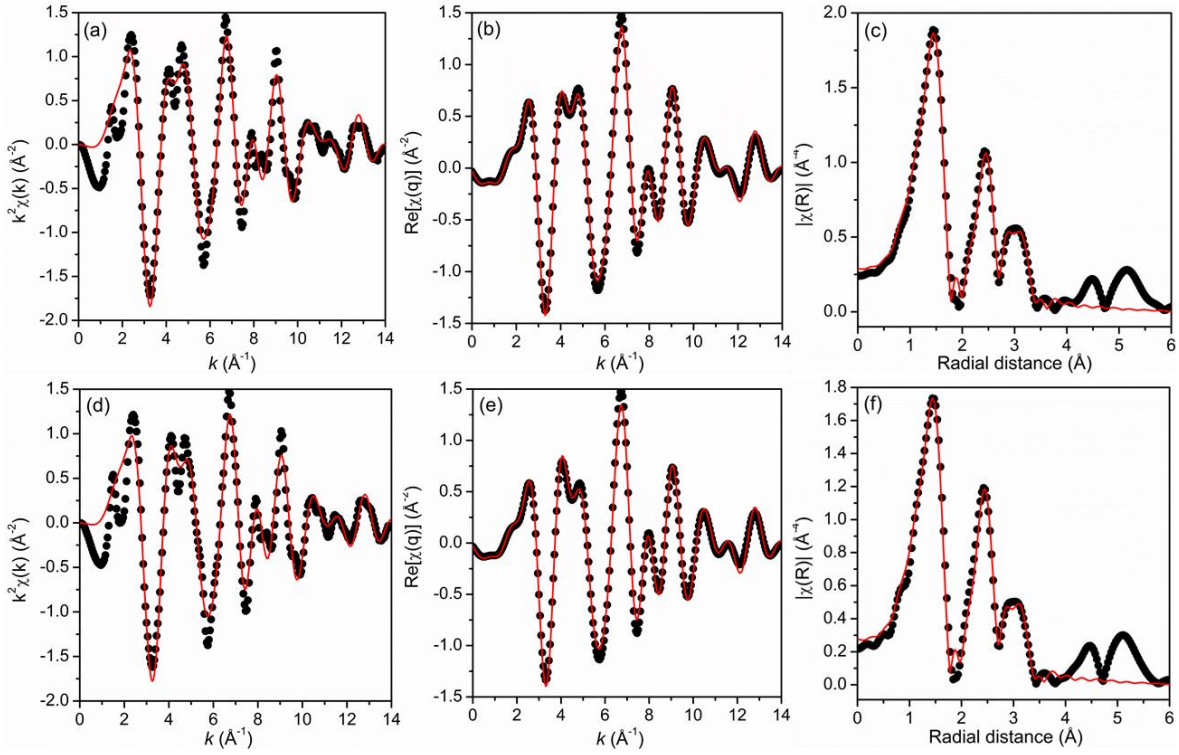

Figure S4: Fits to the *EXAFS spectra shown in Fits are shown in (a) reciprocal (k) space, (b) q-space and (c) the real component of the EXAFS Fourier transform in real space (R) for the $Ca_2Mn_3O_8$ material prepared using the co-precipitation method and (d) reciprocal (k) space, (e) q-space and (f) the real component of the EXAFS Fourier transform in real space (R) for the $Ca_2Mn_3O_8$ material prepared using the hydrothermal method. The black circles represent the observed data and the red line represents the fit.*

Magnetic characterisation

Figures S5, S6 and S7 give the Curie-Weiss and $d(\chi T)/dT$ plots for the $Ca_2Mn_3O_8$ materials prepared by co-precipitation, sol-gel and hydrothermal methods respectively. A clear transition at the Neél temperature, T_N, is seen in all three materials at approximately 60 K in the $d(\chi T)/dT$ plots. Additionally the data clearly deviates away from Curie-Weiss behaviour around 130 K; well above T_N. This transition is far more pronounced in the $d(\chi T)/dT$ plots for the hydrothermal and sol-gel prepared materials. Figure S8 gives AC susceptibility data as a function of frequency. We note that no frequency dependence of the data is observed suggesting that differences between the zero field cooled (ZFC) and field cooled (FC) data do not arise from the evolution of a spin glass-like state.

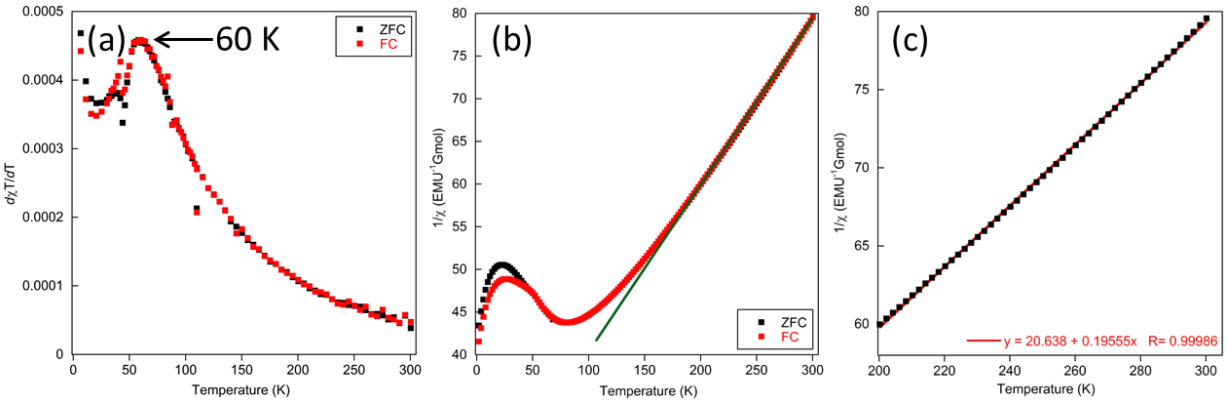

Figure S5: *(a) derivative, dχT/dT vs. temperature data showing T_N at approximately 60 K (b) 1/χ vs. temperature data showing deviation from the Curie-Weiss law (as indicated by the solid green line) at approximately 130 K and (c) linear fit to the Curie-Weiss region between 200 K and 300 K for the zero field cooled data collected for the $Ca_2Mn_3O_8$ material prepared by co-precipitation methods.*

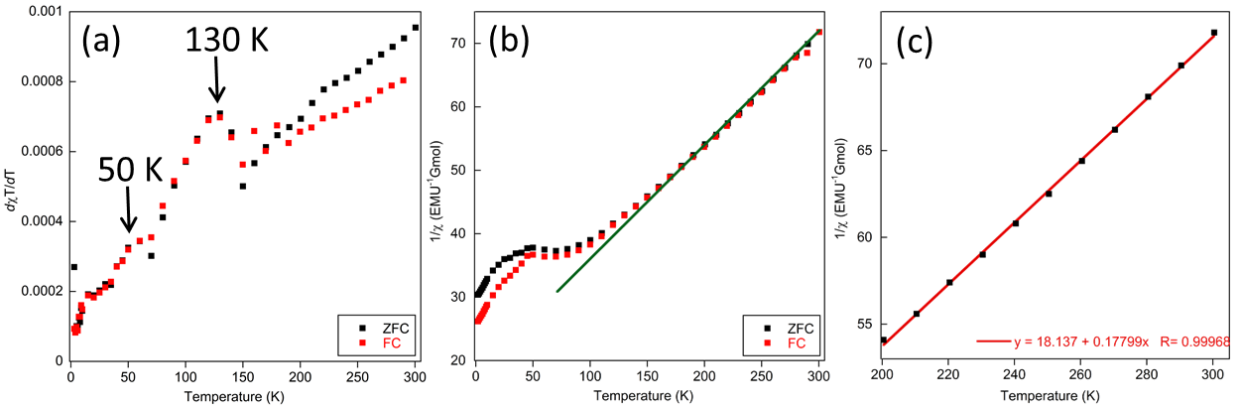

Figure S6: *(a) derivative, dχT/dT vs. temperature data showing T_N at approximately 50 K and clearly indicating a second transition at approximately 130 K (b) 1/χ vs. temperature data showing deviation from the Curie-Weiss law (as indicated by the solid green line) at approximately 130 K and (c) linear fit to the Curie-Weiss region between 200 K and 300 K for the zero field cooled data collected for the $Ca_2Mn_3O_8$ material prepared by sol-gel methods.*

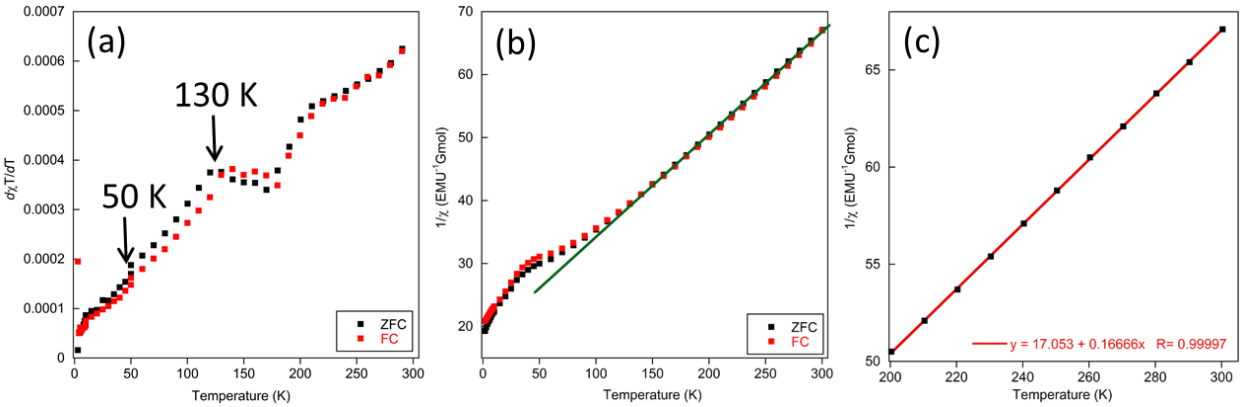

Figure S7: *(a) derivative, dχT/dT vs. temperature data showing T_N at approximately 50 K and clearly indicating a second transition at approximately 130 K (b) 1/χ vs. temperature data showing deviation from the Curie-Weiss law (as indicated by the solid green line) at approximately 130 K and (c) linear fit to the Curie-Weiss region between 200 K and 300 K for the zero field cooled data collected for the $Ca_2Mn_3O_8$ material prepared by hydrothermal methods.*

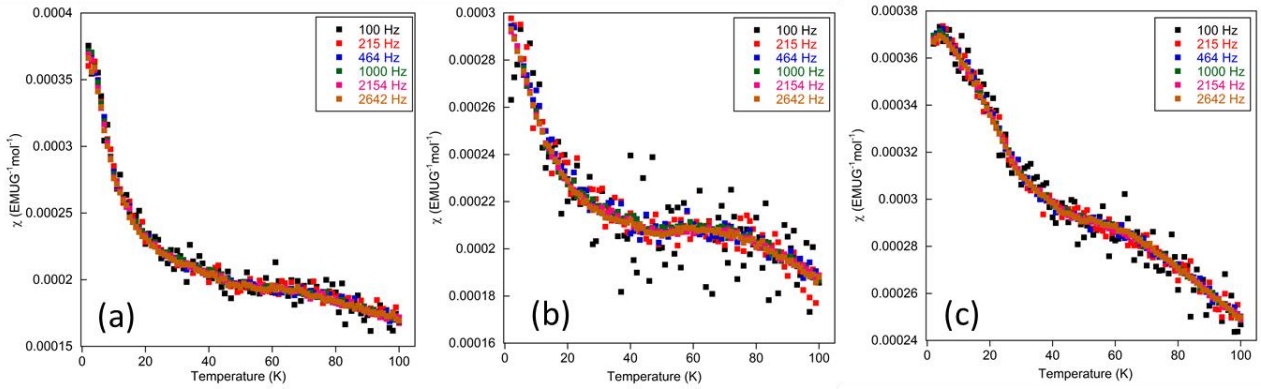

Figure S8: *AC susceptibility data collected as a function of frequency for* $Ca_2Mn_3O_8$ *materials prepared by (a) co-precipitation (b) sol-gel and (c) hydrothermal methods showing no frequency dependence of the suceptibility.*

References

[1] A. C. Larson, R. B. V. Dreele, *Los Alamos National Laboratory Report LAUR* **96**, *86*.

[2] B. H. Toby, *J. Appl. Cryst.* **2001**, *34*, 210.

[3] G. B. Ansell, M. A. Modrick, J. M. Longo, K. R. Poeppelmeier, H. S. Horowitz, *Acta Cryst. B.*, **1982**, *38*, 1795.